The Single-crystal Electron Spin Resonance Spectra of Dichloro- and Dibromo-oxobis(*N,N,N',N'*-tetramethylurea)vanadium(IV); Weak Two-dimensional Exchanging Systems †

Brendan Gahan and Frank E. Mabbs *
Chemistry Department, University of Manchester, Manchester M13 9PL

The single-crystal e.s.r. spectra of $[VOX_2(tmu)_2]$, where X = Cl or Br and tmu = *N,N,N',N'*-tetramethylurea, at *Q*-band frequencies and over the temperature range 300—4.2 K are reported. Unusual fine structure, which does not correlate with the presence of an integral number of strongly interacting vanadium centres, was observed in the range *ca.* 170—120 K. The spectra have been successfully simulated on the basis of a weak isotropic electronic exchange interaction, J_0, within a two-dimensional layer. Parameters used were $g_{\|} = 1.941 \pm 0.002$, $g_{\perp} = 1.979 \pm 0.002$, $A_{\|} = -203 \pm 2$ G, $A_{\perp} = -69 \pm 2$ G, and $J_0 = 130 \pm 2$ G (antiferromagnetic).

Electron paramagnetic resonance measurements on single crystals of undiluted compounds can be extremely useful for probing the electronic structures of transition-metal complexes, particularly when coupled with single-crystal absorption spectra. For an isolated monomeric centre we would expect to observe $(2I + 1)$ hyperfine lines associated with each electronic transition. Such a simple hyperfine pattern is often not observed for a number of reasons. If the paramagnetic ion is part of a discrete polymeric unit, with strong electronic exchange interactions, then each electronic transition will be split into $(2I_{eff.} + 1)$ lines,[1] where $I_{eff.} = nI$ and n = number of equivalent interacting ions. A typical example of this is the dimer $[\{Cu(O_2CMe)_2(H_2O)\}_2]$,[2,3] where seven hyperfine lines are resolvable. However, more commonly when examining undiluted monomeric compounds, no metal hyperfine splittings are observed due to the neighbouring magnetic dipoles causing splittings to such an extent that the hyperfine structure is lost and a broadened single line results.[1] On the other hand, if there is strong electronic exchange over an infinite number of paramagnetic centres, then the hyperfine structure may still be lost, but now line narrowing rather than broadening may result.[1,4-7] A less common situation is that in which the electronic exchange interactions between adjacent paramagnetic centres are comparable to, or slightly less than, the nuclear hyperfine interaction. This situation has been observed in *cis*-$[VO(pbd)_2]$, where pbd = 1-phenylbutane-1,3-dionate, in which the molecules occur as centrosymmetrically related pairs,[8] and in the one-dimensional exchanging system $[NBu^n_4]_2[Cu(mnt)_2]$,[9] where mnt = maleonitriledithiolate. In each of these examples unusual e.s.r. spectra were observed wherein the number of resolved features was not compatible with that expected for any simple discrete small polymeric units containing equivalent interacting centres. For *cis*-$[VO(pbd)_2]$ the spectra were analysed [8] in terms of an isotropic electronic exchange within a dimeric unit, the exchange being greater than the vanadium hyperfine splitting. The e.s.r. spectra at 4.2 K of the copper compound were interpreted on the basis of a one-dimensional system in which the combined isotropic electronic exchange and dipolar interactions were slightly smaller than the copper nuclear hyperfine interaction.[9]

As part of a wider investigation of the electronic structures of MO^{m+} compounds,[10-21] where M = V, Cr, Mo, or W, we now report the single-crystal e.s.r. spectra of $[VOX_2(tmu)_2]$ where X = Cl or Br and tmu = *N,N,N',N'*-tetramethylurea over the temperature range 300—4.2 K. We show that the e.s.r. spectra can be interpreted in terms of an electronic exchange interaction, within a two-dimensional layer, the magnitude of the exchange being similar to that of the vanadium hyperfine interaction.

† *Non-S.I. unit employed*: G = 10^{-4} T.

Experimental

The compounds $[VOX_2(tmu)_2]$ were prepared according to the method of du Preez and Sadie.[22] Crystals were grown as reported previously.[19]

E.s.r. spectra were obtained on oriented (by standard *X*-ray techniques) single crystals over the temperature range 300—4.2 K at *Q*-band frequencies using a Varian E112 spectrometer, by methods previously described.[23] The crystals were cooled using an Oxford Instruments ESR35 continuous flow cryostat fitted with a goniometer so that the cooled crystals could be rotated through 360° in a horizontal plane. Temperature measurement and control was achieved *via* a 0.03% Fe–Au thermocouple and a Harwell DT temperature controller. The crystals were mounted such that spectra could be obtained in the crystallographic a^*c, bc, and a^*b planes.

Results and Discussion

The single crystal e.s.r. spectra of $[VOCl_2(tmu)_2]$ at 298 K consisted of an unresolved line the shape and width of which varied with the orientation of the applied magnetic field. Spectra recorded in the crystallographic a^*c plane showed no change in width (*ca.* 600 G peak to peak) or position as the orientation of the applied magnetic field was altered in this plane. The crystallographic a^*c plane contains the molecular plane perpendicular to the terminal VO direction (see below), and thus the above observation was indicative of axial symmetry in the *g* and hyperfine tensors. Further confirmation of this was provided by the fact that spectra recorded at 298 K in the a^*b (Figure 1) and bc crystallographic planes were identical at corresponding orientations of the applied magnetic field relative to the *b* axis. The e.s.r. signal attained its maximum width (*ca.* 1 800 G) when the applied magnetic field was parallel to the crystallographic *b* axis (molecular *z* axis, see below, $\theta = 0°$), and its minimum width (*ca.* 600 G) when the applied magnetic field was perpendicular to the *b* axis ($\theta = 90°$).

The angular variations of the e.s.r. spectrum at 298 K in the bc, a^*b, and a^*c planes were found to persist at temperatures in the ranges 300—*ca.* 170 and *ca.* 120—4.2 K. However, in the temperature range *ca.* 170—120 K some unusual fine

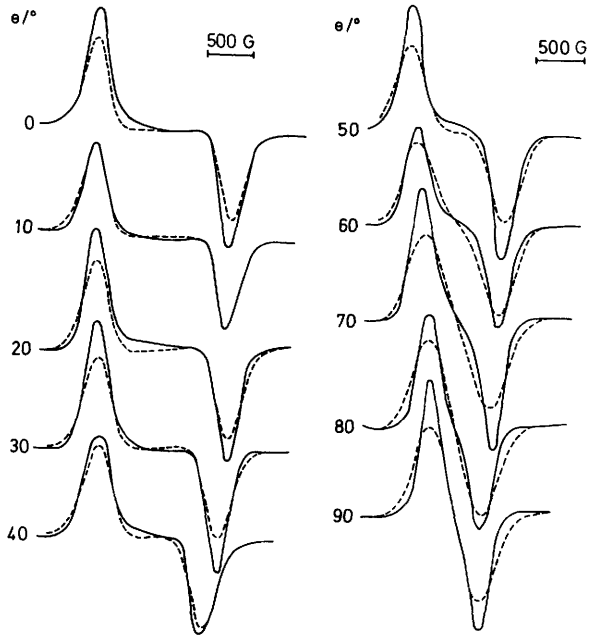

Figure 1. The angular variation of the e.s.r. spectrum of $[VOCl_2(tmu)_2]$ in the a^*b plane at 298 K. θ is the angle of the magnetic field with respect to the b axis as zero. In all diagrams the magnetic field increases from left to right. ——, Experimental; · · · ·, simulated

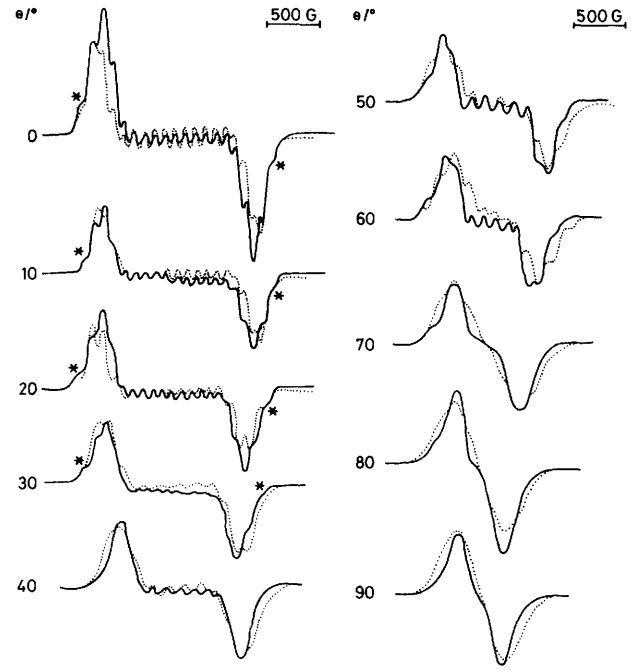

Figure 3. The angular variation of the e.s.r. spectrum of $[VOCl_2(tmu)_2]$ in the a^*b plane at 150 K. θ is measured from the b axis as zero. ——, Experimental; · · · ·, simulated

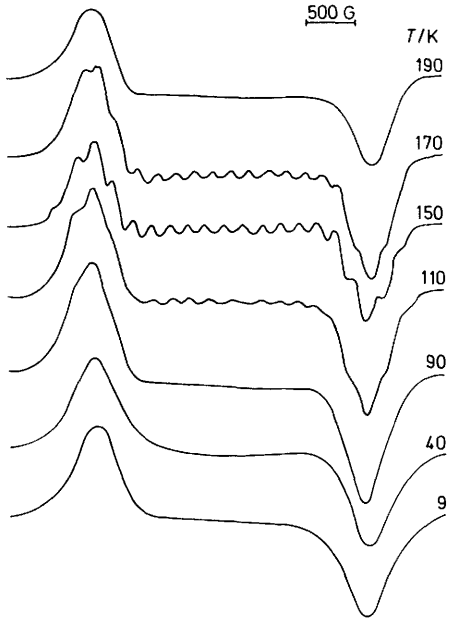

Figure 2. Variation of the e.s.r. spectrum of $[VOCl_2(tmu)_2]$ with temperature with the applied magnetic field parallel to the b axis

structure was superimposed upon the broad featureless room-temperature spectra, see Figure 2. In this temperature range the *total* width of the spectra remained unchanged compared with those obtained at 298 K. The spectra recorded at 150 K in the a^*b plane are in Figure 3. When the applied magnetic field was parallel to the b axis, 19 separate features were observed. The feature at lowest field was a weak shoulder (labelled * in Figure 3) which was followed by three more intense, incompletely resolved features. The previously flat (at 298 K) portion of the spectrum was now resolved into 11 separate features of approximately equal intensity, which upon careful examination were more closely spaced in the centre of the pattern than at either end. This pattern was then followed by features which were an exact reflection of those observed at the low-field end of the spectrum. The e.s.r. spectra showed identical behaviour in the crystallographic bc plane. E.s.r. spectra recorded at X-band frequencies were identical to those obtained at Q-band frequencies at corresponding temperatures and orientations.

The crystal e.s.r. spectra of $[VOBr_2(tmu)_2]$ recorded at Q-band frequencies in the a^*b plane were identical in shape and width to those recorded for $[VOCl_2(tmu)_2]$ at 298 K. However, the single-crystal e.s.r. spectra of $[VOBr_2(tmu)_2]$ are completely invariant with respect to temperature throughout the range 300—4.2 K. Because of their similarity to the spectra of $[VOCl_2(tmu)_2]$ and their invariance with temperature, we assume that the main aspects of the interpretation of these spectra are the same as those applied to the chloro-compound.

Interpretation of Single-crystal Spectra.—The X-ray crystal structure of $[VOCl_2(tmu)_2]$ has been reported by Coetzer.[24] The compound crystallises in the monoclinic space group $C_{2/c}$ and the individual vanadium atoms in the unit cell lie on crystallographically imposed sites of C_2 symmetry. The vanadium–terminal oxygen vectors (V=O) of all the molecules lie parallel to the crystallographic b axis. A diagram of the unit cell is shown in Figure 4. A closer consideration of the crystal structure indicates a substantial ordering of the molecules in the lattice. Figure 5(*a*) and (*b*) show composite diagrams of a number of unit cells projected onto the bc and a^*c planes respectively. The fact that all the V=O vectors are parallel to b, together with a centre of inversion, leads to an effective two-dimensional layer in the bc plane [see Figure 5(*a*)]. The closest vanadium–vanadium separations in this plane are 7.285 Å between molecules related by the inversion centre (resulting in a zigzag chain along the c direction), and 7.870 Å

between molecules related by one unit-cell translation along *b*. There is also a vanadium–vanadium separation of 8.32 Å represented by the short diagonal of the parallelogram formed by four neighbouring V atoms in the *bc* plane. The distance between vanadium atoms in adjacent layers is 9.30 Å.

X-Ray powder diffraction showed that $[VOBr_2(tmu)_2]$ is isomorphous with $[VOCl_2(tmu)_2]$, and thus it is reasonable to assume that it possesses a similar crystal and molecular structure.

By analogy with higher symmetry square-pyramidal oxovanadium(IV) complexes the vanadium–terminal oxygen vector was designated as the molecular *z* axis, which was thus coincident with the crystallographic *b* axis. The molecular *x* axis was defined according to the convention of Belford and co-workers.[8] Because of the packing of the molecules in the unit cell this direction coincides with the crystallographic *c* axis. Thus the molecular *y* axis must then coincide with the crystallographic *a** axis. Since the corresponding molecular axes of all molecules in the crystal are parallel to each other they are all magnetically equivalent at any orientation of the applied magnetic field.

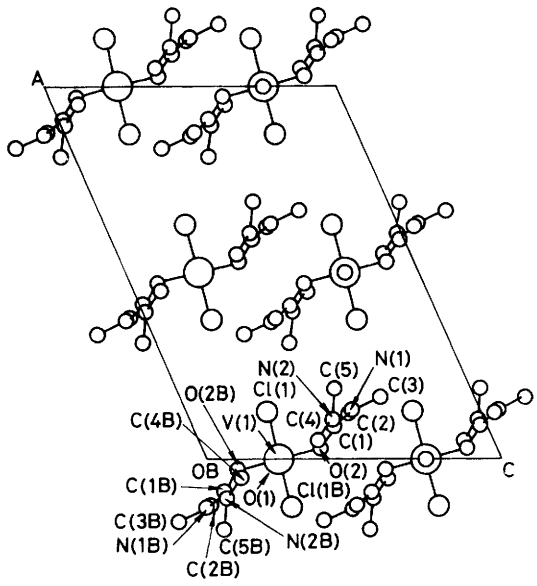

Figure 4. Projection of the unit cell of $[VOCl_2(tmu)_2]$ in the a^*c plane

An initial appraisal of the e.s.r. spectrum of $[VOCl_2(tmu)_2]$ at 150 K and $\theta = 0°$ suggested that it did not arise from a strong ($J > h\nu$) exchange interaction between a small integral number, *n*, of equivalent vanadium atoms, since the maximum number of features observed was not equal to $(2nI + 1)$, where $I = \frac{7}{2}$ for ^{51}V. This suggested that a weak exchange interaction ($J < h\nu$) comparable in size to the vanadium hyperfine splitting could be the cause of the unusual spectrum. The possibilities for the extent of this exchange could be: (*i*) an extended one-dimensional exchange interaction; (*ii*) an extended two-dimensional exchange interaction with *two* close vanadium–vanadium approaches (7.285 and 7.870 Å); (*iii*) an extended two-dimensional exchange interaction with *three* close vanadium–vanadium approaches (7.285, 7.870, and 8.32 Å); and (*iv*) an extended three-dimensional interaction.

Spectrum simulations, based on extension of the one-dimensional model of Soos and co-workers[9] to vanadium, yielded spectra similar to those observed. However they failed to reproduce the weak shoulders (*) at the extremities of the $\theta = 0°$ spectrum at 150 K. In addition it was not possible to reproduce the correct relative intensities of the 11 resolved features in the central part of the spectrum. Simulations based on possibilities (*iii*) and (*iv*) produced extra features at the extremities of the spectra which were not observed experimentally. The possibility (*ii*) provided the best simulations of the spectra, and the method is detailed in the Appendix.

The simulations are based on the statistical occurrence of

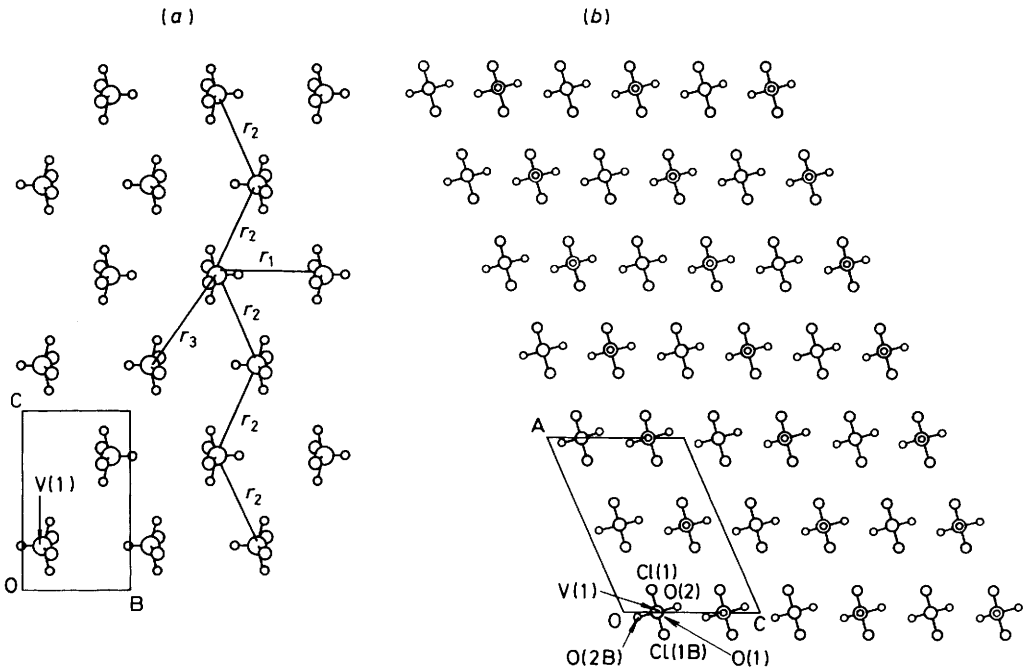

Figure 5. Diagram of a number of adjacent unit cells of $[VOCl_2(tmu)_2]$ in (*a*) the *bc* plane, (*b*) the a^*c plane. Large circles represent vanadium, medium circles chlorine, and smallest circles oxygen

Table 1. Statistical weighting for various segments in a two-dimensional layer of vanadium centres for two close approaches

Length of segments	Statistical weighting	Length of segment	Statistical weighting
(*a*) $N = 1$, $m = 4$		(*b*) $N = 2$, $m = 6$	
$L_1 = L_2 = L_3 = L_4 = 1$	0.3436	$L_1 = L_2 = L_3 = L_4 = L_5 = L_6 = 1$	0.0504
$L_1 = L_2 = L_3 = 1$, $L_4 = 2$ + 3 other possibilities, *i.e.* $L_1 = 2$ or $L_2 = 2$ or $L_3 = 2$ with the L's = 1	0.1718	$L_1 = L_2 = L_3 = L_4 = L_5 = 1$, $L_6 = 2$ + 5 other combinations	0.0378
$L_1 = L_2 = 1$, $L_3 = L_4 = 2$ + 5 other combinations	0.0322	$L_1 = L_2 = L_3 = L_4 = 1$, $L_5 = L_6 = 2$ + 14 other combinations	0.0118
$L_1 = 1$, $L_2 = L_3 = L_4 = 2$ + 3 other combinations	0.0027	$L_1 = L_2 = L_3 = 1$, $L_4 = L_5 = L_6 = 2$ + 19 other combinations	0.0020
$L_1 = L_2 = L_3 = L_4 = 2$	0.0001		

Table 2. Exchange and linewidth parameters for $[VOCl_2(tmu)_2]$ at $T = 150$ K in the a^*b plane; $J_0 = 130 \pm 2.0$ G throughout

θ [a]	$\lvert K(\theta)\rvert$ [b,c]	$D_{zz}^{T}(\theta)$ [c]	$J_{eff.}(\theta)$ [c]	ΔB_{dip} [c]	ΔB_{up} [c,d]	ΔB_{p} [c,d]
0	203.0	−25.1	104.9	50.3	45.0	40.5
10	200.2	−23.1	106.9	50.8	45.0	41.5
20	191.8	−17.3	112.7	51.6	35.0	32.5
30	178.4	−8.4	121.6	54.5	70.0	65.0
40	160.6	2.6	132.6	60.5	90.0	85.0
50	139.6	14.5	144.5	69.2	60.0	65.0
60	116.7	25.6	155.6	78.9	30.0	25.0
70	94.2	34.8	164.8	87.5	50.0	50.0
80	76.3	40.8	170.8	93.4	60.0	60.0
90	69.0	42.9	172.9	95.5	70.0	70.0

[a] In degrees. [b] Absolute value of the effective hyperfine splitting at orientation θ. [c] In Gauss. [d] ±0.3 G.

segments within which the vanadium atoms all have the same instantaneous m_I value and produce an e.s.r. spectrum identical to that of a single centre. The effect of perturbing the energies of these m_I states by an isotropic exchange interaction (J_0), and a nett dipolar exchange interaction [$D_{zz}^{T}(\theta)$, see equation (A24)] by surrounding segments is then considered. In general this interaction splits each m_I line equally in first order, giving extra features in the spectrum, see Table A1. The effective exchange interaction, $J_{eff.}$, at any particular orientation was found by summing the isotropic exchange and the nett dipolar exchange. The various segments incorporated in the simulation described here were those in Table 1. These segments accounted statistically for 65.2% of the total available spectral intensity, and gave rise to 11 648 individual e.s.r. transitions. Second-order effects, which cause uneven splittings depending on the m_I value of the transitions, arising from both the nett exchange interaction and hyperfine interactions were included, although the latter effect is very small at Q-band frequencies. The separation between the weak features (*) at the extremities of the spectra is equal to $7K(\theta) + 4J_{eff.}(\theta)$ [$K(\theta)$ is defined in equation (A5)] in a first-order approximation. However, because of the incomplete resolution of these features, the possibilities of overlapping lines, and second-order effects we decided that it was essential to simulate the spectra. The best fits to the experimental spectra were obtained with $g_{\parallel} = 1.941 \pm 0.002$, $g_{\perp} = 1.979 \pm 0.002$, $A_{\parallel} = -203 \pm 2$ G, $A_{\perp} = -69 \pm 2$ G, and the other parameters in Table 2.

The simulated and experimental spectra at 150 K are compared in Figure 3. This shows that the quality of the simulations is generally very good. In particular the spacings and relative intensities of the central features when $0 \leqslant \theta \leqslant 60°$ are in good agreement. However, although the simulated positions of the features in the wings of the spectra are also in good agreement, their relative intensities sometimes are not. Attempts to improve the relative intensities by changing the additional linewidth parameters which have a very marked effect on the central portion of the spectra (see below), did not result in any improvement without worsening the central portion of the spectrum.

The simulations, in particular the resolution and relative intensities of the central features for $0 \leqslant \theta \leqslant 60°$, were very sensitive to the additional linewidth parameters ΔB_{up} and ΔB_{p} (see Appendix) and to the inclusion of dimensional second-order effects, $H^{(2)}(\theta)$, in the calculation. Without these second-order contributions, the separations between the central features tended to be equal, whereas in the experimental spectra these separations increase away from the geometric centre of the spectrum. The inclusion of the dimensional second-order effects accounted for this aspect, since the absolute value of the second-order term increases as the absolute value of m_I increases, thus giving smaller corrections at the centre of the spectrum ($m_I = \pm\frac{1}{2}$) than at the extremes ($m_I = \pm\frac{7}{2}$). The relative intensities of the central features were very sensitive not only to the size of ΔB_{up}, and ΔB_{p}, but also to the relative magnitudes of these additional linewidths, see Figure 6. A change of as little as 0.5 G in ΔB_{up} and ΔB_{p} was sufficient to alter markedly the relative intensity of the central features. For $0 \leqslant \theta \leqslant 60°$, it was necessary that $\Delta B_{up} \neq \Delta B_{p}$ in order to obtain good simulations. It is possible that attributing different linewidths to different transitions in this manner is in some way compensating for the approximations in the models described above. The values of g and A required for the simulations compare very favourably with those reported by Kuska and Yang [25] for frozen-glass spectra ($g_{\parallel} = 1.941 \pm 0.003$, $g_{\perp} = 1.983 \pm 0.003$, $A_{\parallel} = -193 \pm 1$ G, and $A_{\perp} = -69.2 \pm 7.0$ G).

Three main reasons can be advanced to explain deficiencies in the simulations at various orientations.

(*i*) The assumption that the exchange interaction J_0 may be treated as a perturbation upon the hyperfine interaction, when

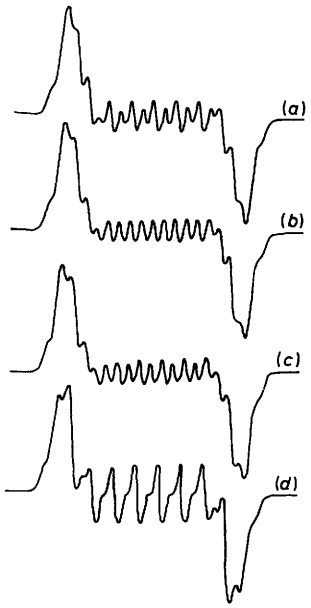

Figure 6. A comparison of the effect of ΔB_{up} and ΔB_p on the simulated e.s.r. spectrum down the *b* axis. The other parameters are those in Table 2 and the text. (*a*) $\Delta B_{up} = 45.0$, $\Delta B_p = 38.5$; (*b*) $\Delta B_{up} = 45.0$, $\Delta B_p = 40.5$; (*c*) $\Delta B_{up} = 45.0$, $\Delta B_p = 41.5$; and (*d*) $\Delta B_{up} = 41.5$, $\Delta B_p = 45.0$ G

the two terms are in fact approximately the same order of magnitude. However, this assumption is essential, otherwise the entire calculation becomes impracticable.

(*ii*) The exclusion of 34.8% of the available spectral intensity from the calculation. Again, this is an unavoidable exclusion, since this remaining intensity is distributed over an infinite number of segments with $N > 2$, each of which has a low statistical weighting. Hence the central segments included in the calculation were truncated at $N = 2$, after which the balance between the additional intensity contributed and the increased computing time becomes unrealistic.

(*iii*) The calculation of the statistical weightings for various combinations of segments was based on the proviso that $|J_0| < |K(\theta)|$. It may be seen from Table 2 that this inequality holds only for $0 \leqslant \theta \leqslant 50°$. For $60 \leqslant \theta \leqslant 90°$, $K(\theta) < J_0 < 2K(\theta)$ and strictly speaking the definition of a segment should change, and hence the statistical weighting should be recalculated. However, the effect of this redefinition is to distribute the intensity more evenly over larger segments [whereas for $J_0 < K(\theta)$, much of the intensity is localised on central monomers and dimers], thus leading to a great increase in computation time for the calculation of a smaller proportion of the overall intensity. Purely for comparison, simulations using the $|J_0| < |K(\theta)|$ definition for the segments are presented for the range $60 \leqslant \theta \leqslant 90°$.

Although the simulated e.s.r. spectra are independent of the sign of $J_{eff.}(\theta)$, they are dependent on the sign of J_0, because $D_{zz}^{T}(\theta)$ calculated from equation (A11) has a sign associated with it. Thus a value of $J_0 = -79.8$ G would give an identical value of $J_{eff.}(\theta)$ for the $\theta = 0°$ spectrum, and hence an identical simulation. However, for $\theta > 0°$ this J_0 value would give different values of $|J_{eff.}(\theta)|$ compared to those for $J_0 = +130$ G, and hence lead to a different angular variation of the simulated spectra. Thus from the angular variation of the spectrum it should be possible to determine the sign of J_0.[26] Within the stated error ranges, $J_0 = +130$ G is a unique value for the interpretation of the present experimental spectra, and it indicates a weak antiferromagnetic exchange between the vanadium centres. This observation contrasts with that of Soos and co-workers [9] who appear to ignore the sign of the dipolar contribution to the effective exchange, and thus conclude that the sign of J_0 cannot be determined. On the other hand Belford and co-workers [8] in their study on $[VO(pbd)_2]$ were able to determine explicitly the sign of J_0 from their simulations, and they reported a ferromagnetic exchange, $J_0 = -200$ G.

In order to simulate the broad featureless spectra which occur outside the temperature range *ca.* 170—120 K it was only necessary to increase both ΔB_{up} and ΔB_p to 150 G. This obliterated the hitherto resolved features giving the simulations in Figure 1 for spectra obtained at 298 K. Because of the invariance of the e.s.r. spectra of $[VOBr_2(tmu)_2]$ with temperature, and their similarity to those of $[VOCl_2(tmu)_2]$ at 298 K, we have made no attempt to simulate them. In view of the isomorphism of these two compounds it is reasonable to suppose that $[VOBr_2(tmu)_2]$ also experiences a two-dimensional electronic exchange interaction of a similar magnitude to that in the chloro-analogue.

As reported for $[VO(pbd)_2]$,[8] the structure and two-dimensional nature of the exchange in the $[VOX_2(tmu)_2]$ compounds makes it difficult to separate direct (metal orbital–metal orbital overlap) from indirect (superexchange) mechanisms for the exchange. Indeed the two-dimensional nature of the exchange makes it seem likely that overall it arises from more than one pathway. However, the close similarity of the exchange interaction in the chloro- and bromo-analogues, as judged from the almost identical overall widths of their e.s.r. spectra, suggests that any indirect pathway for the exchange does not involve the halogeno-groups. The small value of J_0 is however consistent with the large vanadium–vanadium separations for either type of pathway for exchange.

Appendix

In a single crystal of a transition-metal complex, where each metal ion formally has $S = \frac{1}{2}$, the spin Hamiltonian which may include hyperfine interactions, isotropic exchange, and magnetic dipolar exchange can be written as in equation (A1)

$$\mathcal{H} = \sum_i (\beta H \,.\, g \,.\, \hat{S}_i + \hat{S}_i \,.\, A \,.\, \hat{I}_i) + J_0 \sum_i \hat{S}_i \,.\, \hat{S}_{i+1} + \sum_i \hat{S}_i \,.\, D \,.\, \hat{S}_{i+1} \quad \text{(A1)}$$

where J_0 = isotropic exchange parameter between neighbouring sites, D = the tensor representing the classical point dipole–point dipole interaction, H = the applied magnetic field, and $\hat{S}_i$ and $\hat{S}_{i+1}$ are the electronic spin operators of the *i*th and $(i + 1)$th metal site respectively.

Clearly the problem presented by the application of equation (A1) cannot be solved exactly, since the matrices involved have potentially infinite size. A solution to this problem has been given by Soos and co-workers [9] for one-dimensional exchange in $[NBu_4]_2[Cu(mnt)_2]$, where the exchange interactions were treated as perturbations upon the zeroth-order hyperfine levels arising from the application of the first term in equation (A1). In this paper we extend this treatment to the specific case of vanadium(IV) centres ($S = \frac{1}{2}$, $I = \frac{7}{2}$) involved in exchange within a two-dimensional layer, with the exchange interaction being smaller than the hyperfine splitting [*i.e.* $J_0 < K(\theta)$]. The neighbouring vanadium sites in the layer will be *magnetically* inequivalent (although they may be *crystallographically* equivalent) if $M_I(i) \neq M_I(i + 1)$, and thus the layer may be broken down into segments (*N*-mers) of varying lengths within which the sites are magnetically

equivalent. These segments are surrounded by sites, L mers, belonging to segments whose sites have different M_I values. There will thus be a statistical distribution of segments throughout the layer. The simulation of the e.s.r. spectrum reduces to the calculation of (*i*) the statistical distribution of N-mers surrounded by L-mers, (*ii*) the perturbation of the zeroth-order energy levels of each N-mer by exchange interactions with all possible combinations of surrounding L-mers, and (*iii*) the calculation of the relative intensities of the e.s.r. transitions $\Delta M_S = \pm 1$, $\Delta M_I = 0$ which result from (*ii*).

The Statistical Distribution of N-*Mers*.—If all M_I levels on a single centre are thermally accessible the statistical weighting for the combination of a central N-mer surrounded by m L-mers of length $L_1, L_2, \cdots L_m$ is given by equation (A2) where

$$N \,.\, P_N \,.\, P_{L_m} = N \,.\, (2I)^m/(2I+1)^{(m+N-1+L_1+L_2\cdots+L_m)} \quad \text{(A2)}$$

N = the number of sites in the N-mer, P_N = the probability that a segment of length N is surrounded by m sites with different M_I, and P_{L_m} = the probability that the surrounding L-mers simultaneously have members whose M_I values are different from that of the central N-mer.

In the two-dimensional layer found in $[VOCl_2(tmu)_2]$, see Figure 5(*a*), where the neighbours in the chain are alternately staggered, then there may be three possible close approaches (r_1, r_2, and r_3) between neighbouring vanadium centres. Since we subsequently satisfactorily simulated our e.s.r. spectra on the basis of exchange between neighbouring vanadiums, represented by r_1 and r_2, the statistical weightings from equation (A2) for this situation are given in Table 1. The total intensity included in the e.s.r. simulation based on the segments in Table 1 is 62.5%.

Perturbation of the N-*Mers by Surrounding* L-*Mers*.—In the absence of the exchange interaction between neighbouring vanadium atoms, the transition energies between hyperfine levels resulting from the application of equation (A1) to a system with axially symmetric g and A tensors are as in equation (A3) where ν = the applied microwave frequency, H = the applied magnetic field, and θ = the angle between H

$$h\nu = \beta g(\theta)[H + K(\theta) \,.\, M_I + \Delta K(\theta)^{(2)}] \quad \text{(A3)}$$

$$g^2(\theta) = g_\parallel{}^2\cos^2\theta + g_\perp{}^2\sin^2\theta \quad \text{(A4)}$$

$$K^2(\theta) = (A_\parallel{}^2 g_\parallel{}^2\cos^2\theta + A_\perp{}^2 g_\perp{}^2\sin^2\theta)/g^2(\theta) \quad \text{(A5)}$$

$$\Delta K(\theta)^{(2)} = \frac{[A_\parallel{}^2 + K^2(\theta)]A_\perp{}^2[I(I+1) - M_I{}^2]}{4K^2(\theta)\beta g(\theta)H} + \frac{A_\parallel{}^2 - A_\perp{}^2}{[8K^2(\theta)\beta g(\theta)H]}\left[\frac{g_\parallel g_\perp}{g(\theta)}\right]^2 . \sin^2 2\theta \,.\, M_I{}^2 \quad \text{(A6)}$$

and the molecular z axis. Furthermore it can be shown that provided the exchange interaction is a perturbation on the Zeeman and hyperfine interactions, and that $J_0 \ll kT$, then exchange *within* an N-mer does not affect the e.s.r. spectrum, which remains the same as that for a *single* centre.[9] Thus any additional features observed in the e.s.r. spectrum arise from perturbation of the zeroth-order levels due to exchange between N-mers and surrounding L-mers.

The exchange operators in equation (A1) are more complicated for a two-dimensional compared with a one-dimensional system. It is now no longer possible to express the exchange operators for different combinations of N-mers and L-mers in a completely general form.

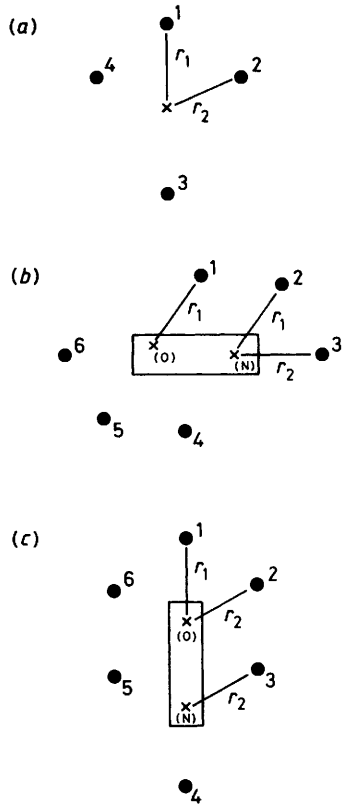

Figure 7. Diagrammatic representation of the two close vanadium–vanadium distances within the two-dimensional layer. (*a*) A central monomer, x, surrounded by monomers, ●; (*b*) and (*c*) the two possible central dimers, x x, surrounded by monomers, ●

For a *central monomer* with two close approaches, r_1 and r_2, see Figure 7(*a*), there are four surrounding members of different segments. When $r_1 \neq r_2$, the dipolar exchange interaction between the N-mer and sites 2 and 4 will be different from the dipolar interaction between the N-mer and sites 1 and 3 at any particular orientation of the applied magnetic field. Thus, assuming the same value of J_0 for the different distances r_1 and r_2, the first-order exchange operator may be written as in equation (A7) and the second-order exchange operator as in equation (A8) where $D_{zz}{}^{(1)}(\theta)$ and $D_{zz}{}^{(2)}(\theta)$ are the truncated

$$V_N(\|) = [J_0 + D_{zz}{}^{(1)}(\theta)](\hat{S}_1{}^z\hat{S}_N{}^z + \hat{S}_N{}^z\hat{S}_3{}^z) + [J_0 + D_{zz}{}^{(2)}(\theta)](\hat{S}_4{}^z\hat{S}_N{}^z + \hat{S}_N{}^z\hat{S}_2{}^z) \quad \text{(A7)}$$

$$V_N(\perp) = \tfrac{1}{2}[J_0 - \tfrac{1}{2}D_{zz}{}^{(1)}(\theta)](\hat{S}_1{}^+\hat{S}_N{}^- + \hat{S}_1{}^-\hat{S}_N{}^+ + \hat{S}_N{}^+\hat{S}_3{}^- + \hat{S}_N{}^-\hat{S}_3{}^+) + \tfrac{1}{2}[J_0 - \tfrac{1}{2}D_{zz}{}^{(2)}(\theta)](\hat{S}_4{}^+\hat{S}_N{}^- + \hat{S}_4{}^-\hat{S}_N{}^+ + \hat{S}_N{}^+\hat{S}_2{}^- + \hat{S}_N{}^-\hat{S}_2{}^+) \quad \text{(A8)}$$

dipolar interaction terms between the N-mer and sites 1 or 3 and sites 2 or 4 respectively [equation (A9)], where r_{ij} = the distance between the ith and jth neighbouring sites and p = the

$$D_{zz}{}^{(1)}(\theta) = \beta g(\theta)(1 - 3\cos^2 p)/r_{ij}{}^3 \quad \text{(A9)}$$

angle between the applied magnetic field and r_{ij}. It should be noted that in structures where the dipolar interactions between the N-mer and site 2, and between the N-mer and site 4 (and similarly for sites 1 and 3), are not always equal at all orientations of the magnetic field then equations (A7) and (A8) must be expanded further.

The application of equation (A7) leads to the first-order correction to the zeroth-order resonance fields, equation (A10) where $F_{L_i} = \langle S_{L_i}S_{L_i}^z|\hat{S}_N^z|S_{L_i}S_{L_i}^z\rangle$ and S_N^z is the

$$H^{(1)}(\theta) = \frac{1}{N}[J_0 + D_{zz}^{(1)}(\theta)][F_{L_1} + F_{L_3}] + \frac{1}{N}[J_0 + D_{zz}^{(2)}(\theta)][F_{L_2} + F_{L_4}] \quad \text{(A10)}$$

z component of the spin operator for *either* the first or last member of the N-mer (segments are symmetric with respect to interchanging the ends since they do not interact in zeroth order).

Equation (A8), the use of closure,[27] and the identities $\hat{S}_j^z = -\frac{1}{2} + \hat{S}_j^+\hat{S}_j^- = \frac{1}{2} - \hat{S}_j^-\hat{S}_j^+$ for $S = \frac{1}{2}$ gives the second-order corrections to the resonance fields, equation (A11) where $C_1 = [J_0 - \frac{1}{2}D_{zz}^{(1)}(\theta)]^2/4K(\theta)$ and $C_2 =$

$$H^{(2)}(\theta) = \frac{C_1}{N}\left(\frac{1}{M_I^N - M_I^{L_1}} + \frac{1}{M_I^N - M_I^{L_3}}\right) + \frac{C_2}{N}\left(\frac{1}{M_I^N - M_I^{L_2}} + \frac{1}{M_I^N - M_I^{L_4}}\right) \quad \text{(A11)}$$

$[J_0 - \frac{1}{2}D_{zz}^{(2)}(\theta)]^2/4K(\theta)$. The terms in parentheses are evaluated as the mean of all combinations of $M_I^{L_i}$ for a fixed value M_I^N, excluding $M_I^{L_i} = M_I^N$.

When a central dimer is considered, Figure 7(*b*) and (*c*), surrounded by six segments it can be seen that if $r_1 \neq r_2$ then the dimer constructed from sites separated by r_1 will have a different nett exchange operator from those constructed from sites separated by r_2. The respective operators $V_N(\|)$ and $V_N(\perp)$ and the first- and second-order corrections to the resonance fields may be written down directly [equations (A13)—(A22)].

$$\text{For } M_I^N = \pm\tfrac{7}{2},\ H^{(2)}(\theta) = \left(\frac{C_1 + C_2}{N}\right)(\pm 0.7408)$$
$$M_I^N = \pm\tfrac{5}{2},\ H^{(2)}(\theta) = \left(\frac{C_1 + C_2}{N}\right)(\pm 0.4143)$$
$$M_I^N = \pm\tfrac{3}{2},\ H^{(2)}(\theta) = \left(\frac{C_1 + C_2}{N}\right)(\pm 0.2238)$$
$$M_I^N = \pm\tfrac{1}{2},\ H^{(2)}(\theta) = \left(\frac{C_1 + C_2}{N}\right)(\pm 0.0714) \quad \text{(A12)}$$

The simulation of the e.s.r. spectra for a two-dimensional layer based on the segments listed in Table 1 and equations (A10), (A12), (A15), (A17), (A20), and (A22) is computationally expensive. This approach generates 29 312 separate transitions and the calculation of the overall spectrum took *ca.* 120 central processor unit (cpu) seconds. We have been able to reduce this computation time, and produce satisfactory spectrum simulations, using the following approximation.

If the component dipolar interactions $D_{zz}^{(1)}(\theta)$ and $D_{zz}^{(2)}(\theta)$ are added to yield a nett dipolar interaction $D_{zz}^{T}(\theta)$ then the nett exchange operators simplify. For a central monomer ($N = 1$), we obtain equations (A23) and (A24) where

---

(*a*) Dimer in Figure 7(*b*)

$$V_N(\|) = [J_0 + D_{zz}^{(1)}(\theta)](\hat{S}_1^z\hat{S}_0^z + \hat{S}_0^z\hat{S}_5^z + \hat{S}_2^z\hat{S}_N^z + \hat{S}_N^z\hat{S}_4^z) + [J_0 + D_{zz}^{(2)}(\theta)](\hat{S}_6^z\hat{S}_0^z + \hat{S}_N^z\hat{S}_3^z) \quad \text{(A13)}$$

$$V_N(\perp) = \tfrac{1}{2}[J_0 - \tfrac{1}{2}D_{zz}^{(1)}(\theta)](\hat{S}_1^+\hat{S}_0^- + \hat{S}_1^-\hat{S}_0^+ + \hat{S}_2^+\hat{S}_N^- + \hat{S}_2^-\hat{S}_N^+ + \hat{S}_0^+\hat{S}_5^- + \hat{S}_0^-\hat{S}_5^+ + \hat{S}_N^+\hat{S}_4^- + \hat{S}_N^-\hat{S}_4^+) + \tfrac{1}{2}[J_0 - \tfrac{1}{2}D_{zz}^{(2)}(\theta)](\hat{S}_6^+\hat{S}_0^- + \hat{S}_6^-\hat{S}_0^+ + \hat{S}_N^+\hat{S}_3^- + \hat{S}_N^-\hat{S}_3^+) \quad \text{(A14)}$$

$$H^{(1)}(\theta) = \frac{1}{N}[J_0 + D_{zz}^{(1)}(\theta)](F_{L_1} + F_{L_2} + F_{L_4} + F_{L_5}) + \frac{1}{N}[J_0 + D_{zz}^{(2)}(\theta)](F_{L_6} + F_{L_3}) \quad \text{(A15)}$$

$$H^{(2)}(\theta) = \frac{C_1}{N}\left(\frac{1}{M_I^N - M_I^{L_1}} + \frac{1}{M_I^N - M_I^{L_2}} + \frac{1}{M_I^N - M_I^{L_4}} + \frac{1}{M_I^N - M_I^{L_5}}\right) + \frac{C_2}{N}\left(\frac{1}{M_I^N - M_I^{L_6}} + \frac{1}{M_I^N - M_I^{L_3}}\right) \quad \text{(A16)}$$

$$\text{For } M_I^N = \pm\tfrac{7}{2},\ H^{(2)}(\theta) = \frac{C_1}{N}(\pm 1.4816) + \frac{C_2}{N}(\pm 0.7408)$$
$$M_I^N = \pm\tfrac{5}{2},\ H^{(2)}(\theta) = \frac{C_1}{N}(\pm 0.8286) + \frac{C_2}{N}(\pm 0.4143)$$
$$M_I^N = \pm\tfrac{3}{2},\ H^{(2)}(\theta) = \frac{C_1}{N}(\pm 0.4476) + \frac{C_2}{N}(\pm 0.2238)$$
$$M_I^N = \pm\tfrac{1}{2},\ H^{(2)}(\theta) = \frac{C_1}{N}(\pm 0.1429) + \frac{C_2}{N}(\pm 0.0714) \quad \text{(A17)}$$

(*b*) Dimer in Figure 7(*c*)

$$V_N(\|) = [J_0 + D_{zz}^{(1)}(\theta)](\hat{S}_1^z\hat{S}_0^z + \hat{S}_N^z\hat{S}_4^z) + [J_0 + D_{zz}^{(2)}(\theta)](\hat{S}_6^z\hat{S}_0^z + \hat{S}_0^z\hat{S}_2^z + \hat{S}_5^z\hat{S}_N^z + \hat{S}_N^z\hat{S}_3^z) \quad \text{(A18)}$$

$$V_N(\perp) = \tfrac{1}{2}[J_0 - \tfrac{1}{2}D_{zz}^{(2)}(\theta)](\hat{S}_1^+\hat{S}_0^- + \hat{S}_1^-\hat{S}_0^+ + \hat{S}_N^+\hat{S}_4^- + \hat{S}_N^-\hat{S}_4^+) + \tfrac{1}{2}[J_0 - \tfrac{1}{2}D_{zz}^{(2)}(\theta)](\hat{S}_6^+\hat{S}_0^- + \hat{S}_6^-\hat{S}_0^+ + \hat{S}_0^+\hat{S}_2^- + \hat{S}_0^-\hat{S}_2^+ + \hat{S}_5^+\hat{S}_N^- + \hat{S}_5^-\hat{S}_N^+ + \hat{S}_N^+\hat{S}_3^- + \hat{S}_N^-\hat{S}_3^+) \quad \text{(A19)}$$

$$H^{(1)}(\theta) = \frac{1}{N}[J_0 + D_{zz}^{(1)}(\theta)](F_{L_1} + F_{L_4}) + \frac{1}{N}[J_0 + D_{zz}^{(2)}(\theta)](F_{L_6} + F_{L_2} + F_{L_5} + F_{L_3}) \quad \text{(A20)}$$

$$H^{(2)}(\theta) = \frac{C_1}{N}\left(\frac{1}{M_I^N - M_I^{L_1}} + \frac{1}{M_I^N - M_I^{L_4}}\right) + \frac{C_2}{N}\left(\frac{1}{M_I^N - M_I^{L_6}} + \frac{1}{M_I^N - M_I^{L_2}} + \frac{1}{M_I^N - M_I^{L_5}} + \frac{1}{M_I^N - M_I^{L_3}}\right) \quad \text{(A21)}$$

For

$$\left.\begin{aligned} M_I^N = \pm\tfrac{7}{2},\ H^{(2)}(\theta) &= \frac{C_1}{N}(\pm 0.7408) + \frac{C_2}{N}(\pm 1.4816) \\ M_I^N = \pm\tfrac{5}{2},\ H^{(2)}(\theta) &= \frac{C_1}{N}(\pm 0.4143) + \frac{C_2}{N}(\pm 0.8286) \\ M_I^N = \pm\tfrac{3}{2},\ H^{(2)}(\theta) &= \frac{C_1}{N}(\pm 0.2238) + \frac{C_2}{N}(\pm 0.4476) \\ M_I^N = \pm\tfrac{1}{2},\ H^{(2)}(\theta) &= \frac{C_1}{N}(\pm 0.0714) + \frac{C_2}{N}(\pm 0.1429) \end{aligned}\right\} \quad (A22)$$

$$V_N(\|) = [J_0 + D_{zz}^{T}(\theta)](\hat{S}_1^z\hat{S}_N^z + \hat{S}_N^z\hat{S}_2^z + \hat{S}_3^z\hat{S}_N^z + \hat{S}_N^z\hat{S}_4^z) \quad (A23)$$

$$V_N(\perp) = \tfrac{1}{2}[J_0 - \tfrac{1}{2}D_{zz}^{T}(\theta)](\hat{S}_1^+\hat{S}_N^- + \hat{S}_1^-\hat{S}_N^+ + \hat{S}_N^+\hat{S}_2^- + \hat{S}_N^-\hat{S}_2^+ + \hat{S}_N^+\hat{S}_3^- + \hat{S}_N^-\hat{S}_3^+ + \hat{S}_N^+\hat{S}_4^- + \hat{S}_N^-\hat{S}_4^+ \quad (A24)$$

$D_{zz}^{T}(\theta) = D_{zz}^{(1)}(\theta) + D_{zz}^{(2)}(\theta)$. The first- and second-order corrections to the resonance fields become (A25) where $J_{eff.}(\theta) = J_0 + D_{zz}^{T}(\theta)$ and (A26) where $C^T = [J_0 - \frac{1}{2}D_{zz}^{T}(\theta)]^2/4K(\theta)$.

$$H^{(1)}(\theta) = \frac{1}{N}[J_{eff.}(\theta)](F_{L_1} + F_{L_2} + F_{L_3} + F_{L_4}) \quad (A25)$$

$$H^{(2)}(\theta) = \frac{C^T}{N}\left(\frac{1}{M_I^N - M_I^{L_1}} + \frac{1}{M_I^N - M_I^{L_2}} + \frac{1}{M_I^N - M_I^{L_3}} + \frac{1}{M_I^N - M_I^{L_4}}\right) \quad (A26)$$

For

$$\left.\begin{aligned} M_I^N = \pm\tfrac{7}{2},\ H^{(2)}(\theta) &= \frac{C^T}{N}(\pm 1.4816) \\ M_I^N = \pm\tfrac{5}{2},\ H^{(2)}(\theta) &= \frac{C^T}{N}(\pm 0.8286) \\ M_I^N = \pm\tfrac{3}{2},\ H^{(2)}(\theta) &= \frac{C^T}{N}(\pm 0.4476) \\ M_I^N = \pm\tfrac{1}{2},\ H^{(2)}(\theta) &= \frac{C^T}{N}(\pm 0.1429) \end{aligned}\right\} \quad (A27)$$

For a central dimer ($N = 2$), the nett operator removes any effective distinction between the situations in Figure 7(*b*) and (*c*) leading to expressions (A28) and (A29). The first- and second-order corrections to the resonance fields become (A30) and (A31).

The first-order splittings generated by these nett operators [equations (A23) and (A28)] and for various segments are shown in Table A1. In all 11 648 transitions are generated by these operators from the segments in Table 1. The computation time for a spectrum simulation is reduced to *ca.* 50 cpu seconds.

The final equation for the resonance fields, $H_R(\theta)$, for each hyperfine line is (A33).

In zeroth order, the $\Delta S_N^z = \pm 1$ transitions have a total intensity given by equation (A34) where $I_N^{(0)}$ has the values $\frac{1}{4}$ for $N = 1$ and $\frac{1}{2}$ for the $S_N = 1$ manifold for $N = 2$ (the $S_N = 0$ manifold make no contribution). Thus the calculated spectrum will be composed of the sum of the transitions at magnetic fields $H_R(\theta)$ given by equation (A33). The relative intensity of each transition will derive from the statistical weight $N \,.\, P_N \,.\, P_{L_m}$ and the $I_N^{(0)}$ contribution from (A34) giving a nett transition intensity as in equation (A35). The final spectrum was calculated as the first derivative of a Gaussian shape function [28] (A36), where H_A = applied magnetic field, $H_R(\theta)$ = the resonance field, T = nett transition intensity, and $\Delta B(\theta)$ = total linewidth at the angle θ. The linewidth was composed of two parts. (*i*) A Van Vleck truncated dipolar linewidth, $\Delta B_d(\theta)$, calculated from [5] equation (A37), where r_{jk} = distance between the jth and kth dipoles, ρ_{jk} = angle between r_{jk} and the applied magnetic field, and $g_{eff.}^{(j)}$ and $g_{eff.}^{(k)}$ are the effective g values for the sites j and k for the particular orientation of the magnetic field.

$$V_N(\|) = [J_0 + D_{zz}^{T}(\theta)](\hat{S}_1^z\hat{S}_0^z + \hat{S}_0^z\hat{S}_2^z + \hat{S}_N^z\hat{S}_3^z + \hat{S}_N^z\hat{S}_4^z + \hat{S}_5^z\hat{S}_N^z + \hat{S}_6^z\hat{S}_0^z) \quad (A28)$$

$$V_N(\perp) = \tfrac{1}{2}[J_0 - \tfrac{1}{2}D_{zz}^{T}(\theta)](\hat{S}_1^+\hat{S}_0^- + \hat{S}_1^-\hat{S}_0^+ + \hat{S}_0^+\hat{S}_2^- + \hat{S}_0^-\hat{S}_2^+ + \hat{S}_N^+\hat{S}_3^- + \hat{S}_N^-\hat{S}_3^+ + \hat{S}_N^+\hat{S}_4^- + \hat{S}_N^-\hat{S}_4^+ + \hat{S}_5^+\hat{S}_N^- + \hat{S}_5^-\hat{S}_N^+ + \hat{S}_6^+\hat{S}_0^- + \hat{S}_6^-\hat{S}_0^+) \quad (A29)$$

$$H^{(1)}(\theta) = \frac{1}{N} \,.\, J_{eff.}(\theta)(F_{L_1} + F_{L_2} + F_{L_3} + F_{L_4} + F_{L_5} + F_{L_6}) \quad (A30)$$

$$H^{(2)}(\theta) = \frac{C^T}{N}\left(\frac{1}{M_I^N - M_I^{L_1}} + \frac{1}{M_I^N - M_I^{L_2}} + \frac{1}{M_I^N - M_I^{L_3}} + \frac{1}{M_I^N - M_I^{L_4}} + \frac{1}{M_I^N - M_I^{L_5}} + \frac{1}{M_I^N - M_I^{L_6}}\right) \quad (A31)$$

For

$$\left.\begin{aligned} M_I^N = \pm\tfrac{7}{2},\ H^{(2)}(\theta) &= \frac{C^T}{N}(\pm 2.2224) \\ M_I^N = \pm\tfrac{5}{2},\ H^{(2)}(\theta) &= \frac{C^T}{N}(\pm 1.2429) \\ M_I^N = \pm\tfrac{3}{2},\ H^{(2)}(\theta) &= \frac{C^T}{N}(\pm 0.6714) \\ M_I^N = \pm\tfrac{1}{2},\ H^{(2)}(\theta) &= \frac{C^T}{N}(\pm 0.2143) \end{aligned}\right\} \quad (A32)$$

$$H_R(\theta) = H_0 - K(\theta)M_I^N - \Delta K^{(2)}(\theta) + H^{(1)}(\theta) + H^{(2)}(\theta) \quad (A33)$$

$$I_N^{(0)} = 2^{-N}\sum_{S_N} \tfrac{1}{3}S_N(S_N + 1)(2S_N + 1) \quad (A34)$$

$$T = N \,.\, P_N \,.\, P_{L_m} \,.\, I_N^{(0)} \quad (A35)$$

$$\frac{dT(H_A)}{dH_A} = \frac{8T[H_A - H_R(\theta)]}{[\Delta B(\theta)]^3} \,.\, \exp\left\{\frac{-2[H_A - H_R(\theta)]^2}{[\Delta B(\theta)]^2}\right\} \quad (A36)$$

Table A1. Splitting patterns for the two-dimensional nett operator with two close approaches; $\omega = \frac{1}{N}(F_{L_1} + F_{L_2} + F_{L_3} + F_{L_4} + F_{L_5} + F_{L_6})$

Segments	Exchange splitting within each hyperfine line, $\omega J_{\text{eff.}}(\theta)$	Relative intensities within each hyperfine line
$N = 1, L_1 = L_2 = L_3 = L_4 = 1$	$-2, -1, 0, +1, +2$	1 : 4 : 6 : 4 : 1
$N = 1, L_1 = 2, L_2 = L_3 = L_4 = 1$	$-2, -\frac{3}{2}, -1, -\frac{1}{2}, 0, +\frac{1}{2}, +1, +\frac{3}{2}, +2$	1 : 2 : 4 : 6 : 6 : 6 : 4 : 2 : 1
$N = 1, L_1 = L_2 = 2, L_3 = L_4 = 1$	$-2, -\frac{3}{2}, -1, -\frac{1}{2}, 0, +\frac{1}{2}, +1, +\frac{3}{2}, +2$	1 : 4 : 8 : 12 : 14 : 12 : 8 : 4 : 1
$N = 1, L_1 = L_2 = L_3 = 2, L_4 = 1$	$-2, -\frac{3}{2}, -1, -\frac{1}{2}, 0, +\frac{1}{2}, +1, +\frac{3}{2}, +2$	1 : 6 : 16 : 26 : 30 : 26 : 16 : 6 : 1
$N = 2, L_1 = L_2 = L_3 = L_4 = L_5 = L_6 = 1$	$-\frac{3}{2}, -1, -\frac{1}{2}, 0, +\frac{1}{2}, +1, +\frac{3}{2}$	1 : 6 : 15 : 20 : 15 : 6 : 1
$N = 2, L_1 = 2, L_2 = L_3 = L_4 = L_5 = L_6 = 1$	$-\frac{3}{2}, -\frac{5}{4}, -1, -\frac{3}{4}, -\frac{1}{2}, -\frac{1}{4}, 0, +\frac{1}{4}, +\frac{1}{2}, +\frac{3}{4}, +1, +\frac{5}{4}, +\frac{3}{2}$	1 : 2 : 6 : 10 : 15 : 15 : 30 : 15 : 15 : 10 : 6 : 2 : 1
$N = 2, L_1 = L_2 = 2, L_3 = L_4 = L_5 = L_6 = 1$	$-\frac{3}{2}, -\frac{5}{4}, -1, -\frac{3}{4}, -\frac{1}{2}, -\frac{1}{4}, 0, +\frac{1}{4}, +\frac{1}{2}, +\frac{3}{4}, +1, +\frac{5}{4}, +\frac{3}{2}$	1 : 4 : 10 : 20 : 31 : 40 : 44 : 40 : 31 : 20 : 10 : 4 : 1

$$[\Delta B_d(\theta)]^2 = \tfrac{3}{4} g_{\text{eff.}}^{(j)} g_{\text{eff.}}^{(k)} \beta^2 S(S+1) \sum_{j,k} [(1 - 3\cos^2\rho_{jk})^2 / r_{jk}^6] \quad \text{(A37)}$$

The summation did not include the dipolar interaction between neighbouring centres in the chain since this has been included in the exchange operator. (*ii*) An additional linewidth parameter was added to $\Delta B_d(\theta)$ to yield the final $\Delta B(\theta)$. This allowed a different value to be attributed to unperturbed ($\omega \neq 0$), ΔB_{up}, and perturbed ($\omega = 0$), ΔB_p, hyperfine lines.[9] No specific angular dependence was attributed to these extra linewidth parameters.

Acknowledgements

We thank the S.E.R.C. for financial support. Computations were performed on the University of Manchester Regional Computer Centre ICL 1900/CDC 7600 Joint System. Diagrams of the crystal structures were obtained using PLUTO78 from the Cambridge Crystallographic Files.

References

1 A. Abragam and B. Bleaney, ' Electron Paramagnetic Resonance of Transition Ions,' Clarendon Press, Oxford, 1970.
2 B. Bleaney and K. D. Bowers, *Philos. Mag.*, 1952, **43**, 372; *Proc. R. Soc. London, Ser. A*, 1952, **214**, 451.
3 H. Abe and J. Shimada, *Phys. Rev.*, 1953, **90**, 316; *J. Phys. Soc., Jpn.*, 1957, **12**, 1255.
4 C. J. Gorter and J. H. Van Vleck, *Phys. Rev.*, 1947, **72**, 1128.
5 J. H. Van Vleck, *Phys. Rev.*, 1948, **74**, 1168.
6 P. W. Anderson and P. R. Weiss, *Rev. Mod. Phys.*, 1953, **25**, 269.
7 Z. G. Soos, R. T. McGregor, T. T. P. Cheung, and A. J. Silverstein, *Phys. Rev. B*, 1977, **16**, 3036.
8 G. D. Simpson, R. L. Belford, and R. Biagioni, *Inorg. Chem.*, 1978, **17**, 2424.
9 K. W. Plumlee, B. M. Hoffmann, J. A. Ibers, and Z. G. Soos, *J. Chem. Phys.*, 1975, **63**, 1926.
10 P. M. Boorman, C. D. Garner, F. E. Mabbs, and T. J. King, *J. Chem. Soc., Chem. Commun.*, 1974, 663.
11 C. D. Garner, I. H. Hillier, F. E. Mabbs, and M. F. Guest, *Chem. Phys. Lett.*, 1975, **32**, 224.
12 C. D. Garner, I. H. Hillier, J. Kendrick, and F. E. Mabbs, *Nature (London)*, 1975, **258**, 138.
13 C. D. Garner, J. Kendrick, P. Lambert, F. E. Mabbs, and I. H. Hillier, *Inorg. Chem.*, 1976, **15**, 1287.
14 C. D. Garner, L. H. Hill, F. E. Mabbs, D. L. McFadden, and A. T. McPhail, *J. Chem. Soc., Dalton Trans.*, 1977, 853, 1202.
15 C. D. Garner, I. H. Hiller, F. E. Mabbs, C. Taylor, and M. F. Guest, *J. Chem. Soc., Dalton Trans.*, 1976, 2258.
16 C. D. Garner, P. Lambert, F. E. Mabbs, and T. J. King, *J. Chem. Soc., Dalton Trans.*, 1977, 1191.
17 C. D. Garner, N. C. Howlader, F. E. Mabbs, P. M. Boorman, and T. J. King, *J. Chem. Soc., Dalton Trans.*, 1978, 1350.
18 C. D. Garner, N. C. Howlader, F. E. Mabbs, A. T. McPhail, and K. D. Onan, *J. Chem. Soc., Dalton Trans.*, 1978, 1848.
19 D. Collison, B. Gahan, C. D. Garner, and F. E. Mabbs, *J. Chem. Soc., Dalton Trans.*, 1980, 667.
20 L. H. Hill, N. C. Howlader, F. E. Mabbs, M. B. Hursthouse, and K. M. Abdul Malik, *J. Chem. Soc., Dalton Trans.*, 1980, 1475.
21 B. Gahan, N. C. Howlader, and F. E. Mabbs, *J. Chem. Soc., Dalton Trans.*, 1981, 142.
22 J. G. H. du Preez and D. Sadie, *Inorg. Chim. Acta*, 1967, **1**, 202.
23 C. D. Garner, P. Lambert, F. E. Mabbs, and J. K. Porter, *J. Chem. Soc., Dalton Trans.*, 1972, 320.
24 J. Coetzer, *Acta Crystallogr., Sect. B*, 1970, **26**, 872.
25 H. A. Kuska and Pang-Hsiong Yang, *Inorg. Chem.*, 1974, **13**, 1090.
26 D. Collison, B. Gahan, and F. E. Mabbs, following paper.
27 C. Cohen-Tannondji, B. Diu, and F. Lalse, ' Quantum Mechanics,' Wiley, New York, 1977, vol. II, p. 1104.
28 A. Carrington and A. D. MacLachlan, ' Introduction to Magnetic Resonance,' Harper and Row, London, 1967.

Received 4th October 1982; *Paper* 2/1708